Romanian Reports in Physics **XX**, XYZ (2017)

LEFT-HANDED BEHAVIOR OF THE NANOCRYSTALINE FERROMAGNETIC MICROWIRES

G. ABABEI, I.-I. MURGULESCU, S. CORODEANU, V. DOBREA, N. LUPU

National Institute for Research and Development for Technical Physics; 47 Mangeron Boulevard, P.O.Box 833, RO-700050 Iaşi, Romania, E-mail: gababei@phys-iasi.ro; imurgulescu@phys-iasi.ro; scorodeanu@phys-iasi.ro; dobrea@phys-iasi.ro; nicole@phys-iasi.ro

Received

Abstract. Left-handed behavior of $Fe_{73.5}Cu_1Nb_3Si_{13.5}B_9$ (at.%) nanocrystaline ferromagnetic microwires arranged in parallel configurations as free-standing systems in order to develop new metastructures for GHz shielding applications were studied. Microwires with metallic diameters of 60 μm were obtained by cold-drawing process followed by annealing at 500^{o}C for 1 h. The left-handed behavior of the metastructures was investigated in the frequency range 8.2 ÷ 12.4 GHz and confirmed by simulations using the Nicolson-Ross-Weir analytical method. The variation of the interwire distance proves to be a useful tool to obtain metastructures with suitable left-handed characteristics for GHz applications.

Key words: microwires; nanocrystalline structures; shielding; metastructures.

1. INTRODUCTION

Given the exponential growth of the number of electrical and electronic equipments present in everyday life, the problem of electromagnetic pollution became a major concern. For different industries such as automotive, marine or aerospace, the electromagnetic fields' influence represents a problem of operation security. Electromagnetic shielding aims to reduce the propagation of the electromagnetic waves and is based on the use of a screen, a barrier that separates the space into two areas and influences the propagation of the electromagnetic waves from one area to another [1-5]. The shielding mechanism of the electromagnetic shield is determined by the electric/magnetic characteristics of the material from which it is made (electrical conductivity, magnetic permeability, dielectric permittivity, etc.) and the geometric characteristics (shape, thickness, cut-outs, etc.) as well. A special category of the absorbent materials is represented by metamaterials. A metamaterial is considered an electromagnetic absorber with negative values of the dielectric permittivity, ε, and magnetic permeability, μ. These materials are called in the literature "left-handed mediums"/"artificial absorbents with left-handed properties" or simple "metastructures"/"metamaterial" [6-10]. Recently, the properties of ferromagnetic microwires have been

investigated intensively to develop metastructures for high frequency shielding applications [11-15]. Ferromagnetic microwires have attracted significant attention in the development of metastructures for high-frequency shielding applications due to their unique properties like high magnetic permeability, special anisotropy and domain structure. The high magnetic permeability allows them to effectively guide and confine magnetic fields. This property is crucial for shielding applications as it enhances the material's ability to absorb and dissipate electromagnetic energy. Thune ferromagnetic microwires are suitable for protecting sensitive electronic components from high-frequency electromagnetic interference. Their special anisotropy and domain structure which can be controlled during fabrication allows for the design of metastructures with specific magnetic responses, optimizing them for particular shielding needs. The fabrication processes for ferromagnetic microwires, such as rapid solidification and drawing techniques, are scalable and cost-effective, making them viable for large-scale production of high-frequency shielding materials [16-19]. Engineering a negative dielectric response using ferromagnetic microwires involves carefully designing their geometric arrangement for metamaterials design with negative permittivity or permeability, which are essential for high-frequency shielding applications.

The aim of this paper is to report our latest experimental and theoretical results on the left-handed properties of $Fe_{73.5}Cu_1Nb_3Si_{13.5}B_9$ (at.%) nanocrystaline ferromagnetic microwires arranged in parallel configurations, as free-standing systems, in order to develop new metastructures for GHz shielding applications.

2. MATERIALS AND METHODS

The amorphous as-cast precursor microwires were prepared by in-rotating-water spinning method.

$Fe_{73.5}Cu_1Nb_3Si_{13.5}B_9$ (at. %) microwires with metallic diameters of 60 μm were obtained by cold-drawing process, by successive reductions of the metallic diameter of an amorphous as-cast precursor microwire with the initial diameter D = 90 μm using an in-house developed device. The schematic representation of cold-drawing process is indicated in Fig.1.

Shortly, the cold-drawing process is a manufacturing technique used to produce thin wire with a precise and smooth finish by pulling the material through a die without applying heat. This process is commonly used for reductions of the metallic diameter of ferromagnetic microwires. The amorphous as-cast precursor microwire was cleaned to remove any surface impurities or scale. This ensures a clean surface for the drawing process and prevents defects. The leading end of the precursor microwire is tapered or "pointed" to facilitate its entry into the drawing die. Lubricant oil was applied on microwire’s surface in order to reduce friction between the material and the die. The pointed-end is threaded through a drawing

die, which has an opening smaller than the original diameter of the material. The material is then pulled (drawn) through the die using a drawing machine, reducing its diameter and increasing its length. For significant diameter reduction, multiple drawing passes through progressively smaller dies are required.

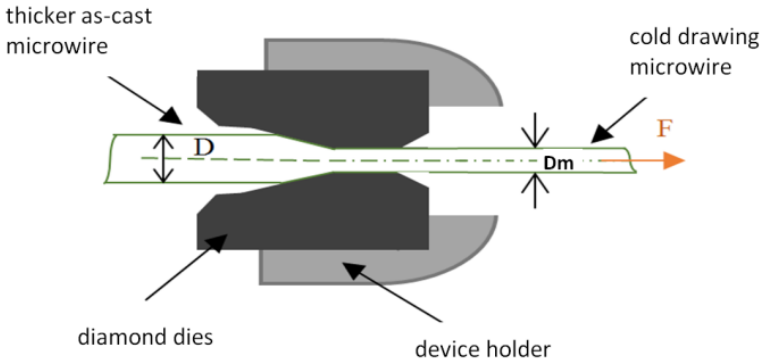

Fig. 1. Schematic representation of cold-drawing process (D – the initial diameter of the as-cast precursor microwire, D_m – the final diameter of the microwire, F – the drawing force direction.

The nanocrystalline structure of the cold drawing microwires (CDMWs) was induced by annealing at 500^{o}C for 1 h, in an oven with controlled temperature and inert gas atmosphere to avoid oxidation. The reason of inducing a monocrystalline structure is that the magnetic permeability at high frequencies of such microwires is enhanced by the presents of nanocrystals with the diameters in the range of 10-25 nm, embedded in an amorphous matrix. The annealing temperature was chosen based on our priori studies of Fe-based microwires magnetically properties [20].

The dimensions of the nanocrystals were investigated by high resolution transmission electron microscopy (TEM), using a Libra200MC microscope (Carl Zeiss, Oberkochen, Germany) at operating at 200 kV. Sample for TEM investigation was prepared by focus ion beam TEM lamella preparation method.

The magnetic properties of the as-cast microwires and (cold drawing nanocrystalline microwires) CDNMWs were investigated by using a flux-metric method, designed and manufactured in-house.

CDNMWs were cut and fixed at their ends, in parallel arrangement and constant inter-wire distance (d= 1 mm and d= 3 mm), on a commercial Teflon sheet holder with a dielectric permittivity ε_{rT} = 2.02 and a thickness g= 0.3 mm. the wires was embedded in a thin layer of a commercial epoxy resin with dielectric permittivity closer to Teflon sheet in order to reduce the microwave scattering at resin-support interface. A microwire length of L = 0.8 cm was used. The inter-wire distance (called as the lattice period) was chosen smaller than the microwave-guide electromagnetic wavelength Λ_g = 4 cm at 10 GHz, in order to satisfy the geometrical conditions of metastructures [19].

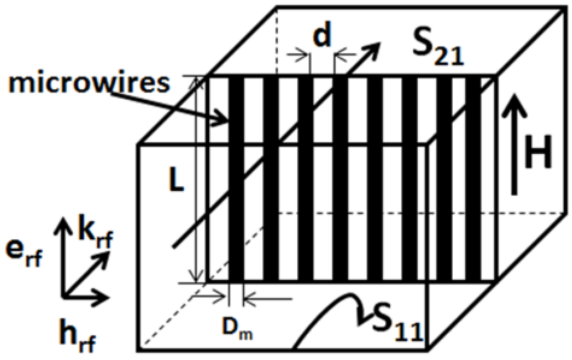

Fig. 2. Schematic representation of microwire's position inside of the microwave guide.

The metastructure was fixed inside of the microwave-guide in the position where the incident microwave electric field, e_{rf}, have maximum value, is parallel and in-plane with the microwires axis, while the microwave magnetic field, h_{rf}, and the propagation vector, k_{rf}, of the microwave field are both out of plane and perpendicular to the CDNMWs axis, as shown in Fig. 2. The orientation of the microwires relative to the incident electromagnetic field influences the dielectric permittivity. Vertical alignment often enhances interaction with the electric field component, leading to stronger resonant effects.

The microwave guide was connected to PNA-VNA L5230 Vector Network Analyzer (Agilent, Santa Clara, United States) emission/reception ports. The TE_{10} dominant mode propagation inside of microwave guide assures a controlled environment. Short-Open-Load-Through (SOLT) calibration of the set-up, in the frequency range 8.2 ÷ 12.4 GHz using a commercial X-band calibration kit was performed before connections of the X-band microwave guide. The SOLT calibration is a widely used method in vector network analysis to calibrate a VNA. This calibration technique is essential for accurate measurement of S-parameters.

The left-handed behavior of the free standing Fe-based CDNMWs based metastructure, have been studied using a WR-90 type X-band microwave guide in the frequency range 8.2 ÷ 12.4 GHz by measuring the reflection, $S_{11}(dB)$ and $S_{22}(dB)$, and the transmission, $S_{21}(dB)$ and $S_{12}(dB)$, respectively, coefficients of the metastructure.

External d.c. magnetic fields, H, were applied using a Helmholtz solenoid system parallel to the long axis of the microwires, in the range of 0 to 32 kA/m.

Negative dielectric response can be engineered by controlling the geometrical characteristics of the microwires arrangement, due to the fact that the periodic metallic structures have plasma-resonance behavior in the microwave frequencies

range, with f_P = 15.1 GHz for d = 3 mm and f_P = 49.6 GHz for d = 1 mm, respectively. At plasma-resonance, the microwires exhibit resonances where the conduction electrons oscillate collectively, leading to a negative dielectric response [21-23].

The left-handed behavior was confirmed by computing the real term of the magnetic permeability, μ^r_{NRW}, and the real term of the dielectric permittivity, ε^r_{NRW}, of the developed metastructures, by using the Nicolson-Ross-Weir analytical method (NWR) [24-30]. The NRW analytical method is a well-established technique for determining the complex permittivity and permeability of materials from S-parameter measurements. This method is widely used in the field of microwave engineering and material science to characterize the electromagnetic properties of metamaterials.

From the measured *S*-complex parameters, the reflection coefficient, *Γ*, is calculated using equation:

$$\Gamma = \frac{S_{11} + S_{22} \pm \sqrt{\left(S_{11} + S_{22}\right)^2 - 4\left(S_{11}S_{22} - S_{21}S_{12}\right)}}{2} \tag{1}$$

where S_{ij} is the complex *S*-parameter form $S_{ij} = S_{ij}^r - iS_{ij}^{img}$ with *i,j= 1 or 2*.

The normalized impedance, *Z*, and propagation constant, *γ*, are calculated using equation:

$$Z = \frac{\left(1+\Gamma\right)}{\left(1-\Gamma\right)} \tag{2}$$

$$\gamma = \frac{1}{b}\ln\left(\frac{1}{T}\right) \tag{3}$$

where *b* is the total thickness of the sample, $b = g + 2D_m$, while *T* is the transmission coefficient, $T = \left|S_{21}\right|^2$.

The complex permittivity and permeability are calculated from *Z* and *γ* using equations:

$$\varepsilon = \varepsilon_{NRW}^{r} - i\varepsilon_{NRW}^{img} = \left(\frac{\gamma}{j\omega\mu_0 Z} \right)^2 \tag{4}$$

$$\mu = \mu_{NRW}^{r} - i\mu_{NRW}^{img} = \frac{Z}{Z_0} \tag{5}$$

where ε_{NRW}^{r} is the real part, and ε_{NRW}^{img} is the imaginary part, respectively, of the dielectric permittivity; while μ_{NRW}^{r} is the real part, and μ_{NRW}^{img} is the imaginary part, respectively, of the magnetic permeability; Z_0 is the impedance of free space, ω is the angular frequency, and μ_0 is the magnetic permeability of free space.

3. RESULTS AND DISCUSSINS

The annealing of cold drawing microwires at 500^0C determined a nanocrystalline structure of metallic microwire. The TEM image of the annealed CDNMWs microstructure shown in Fig. 3 indicated the presence of nanograins with ~15 nm in diameters, embedded in the amorphous matrix.

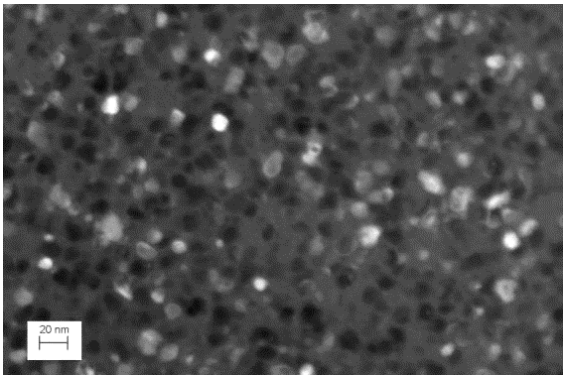

Fig. 3. TEM image of the annealed CDNMWs microstructure.

The magnetic hysteresis loops of the microwires are presented in Fig. 4. The as-cast microwire have a soft magnetic behavior (black curve) with the coercive field below 1 A/m and saturation magnetization, $\mu_0 M_s$ ~ 1.15 T. After cold drawing, the microwires with the metallic diameter D_m = 60μm exhibits a significant increase (red curve) of the coercive field (to ~0.5 kA/m), most probable

due to the internal stresses induced by the mechanical deformation during the cold drawing process. The thermal annealing of the cold-drawn microwires reduces the coercive field (green curve) to values similar with those measured for the as-cast microwires, while the saturation magnetization slightly increases, $\mu_0 M_s \sim 1.25$ T.

The magnetic permeability variation with the external applied magnetic field is shown in Fig. 5. The permeability reaches its maximum for the CDNMWs with $\mu_{r\ CDNMWs} \sim 7.3x10^3$, while the magnetic permeability for the as-cast microwires is $\mu_{r\ as\text{-}cast} \sim 4.9x10^3$. The increase of the magnetic permeability for the nanocrystalline cold-drawn microwires is related to the formation of the suitable nanocrystalline structure after annealing at 500^0C for 1 h.

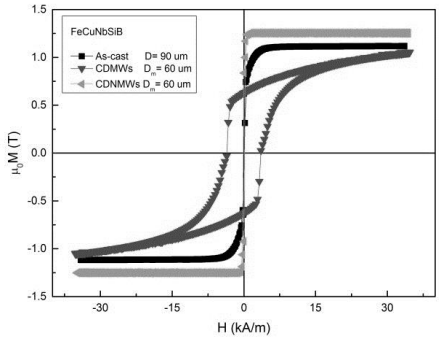

Fig. 4. Magnetic hysteresis loops for the as-cast and cold drawn microwires, before and after annealing.

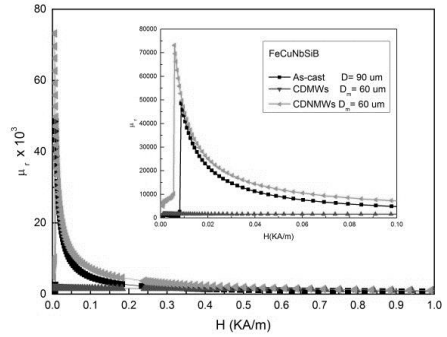

Fig. **5**. Magnetic permeability of the as-cast and cold drawn microwires, before and after annealing.

The high frequencies behaviors of microwires are presented in the frame of Fig. 6 as fallows: Fig. 6 (a) shows the absorption frequency dependence calculated

using reflexion, S_{11}, (Figure 6b) and transmission, S_{21}, (Figure 6c) coefficients measured for the CDNMWs -based metastructure, using the equation:

$$Abs. = 1 - 10^{S_{11}/10} - 10^{S_{21}/10} \quad (6)$$

In the absence of the external magnetic field, *H*, the metastructures with the inter-wire distance of d = 1 mm present a microwave absorption window of about 2 GHz, while the metastructures with the inter-wire distance of d = 3 mm present a microwave absorption window of about 3 GHz. Both absorption windows have the central frequency at about 9.7 GHz. In the presence of the magnetic field, the absorption window is slightly increased with 1 GHz and the central frequencies are shifted to higher frequencies with about 200 MHz. The microwave absorption amplitude of the metastructure with inter-wires distance of d= 3 mm is higher compared with that of the metastructure with the inter-wires distance of d= 1 mm. That behavior may be due to the increasing of dipole effect of microwires and decreasing of dynamic magnetic interactions induced by the electrical components of the incident microwave field. Optimal spacing is critical for achieving a desired negative dielectric response because the distance between microwires affects the coupling between adjacent wires, each short wires behaving like a small dipole. This dipole effect is the reason of the peaks visible to high frequency values on the absorption curves, mainly for interwires distance d= 3mm.

Fig.7 presents the real terms of calculated frequency dependence for ε^{r}_{NRW} (a) and μ^{r}_{NRW} (b) of the metastructure based on CDNMWs with the metallic diameter D_m = 60 μm, using equation (4-5). The measured reflexion, S_{11}, and transmission, S_{21}, coefficients are input values. The imaginary terms of dielectric permittivity and magnetic permeability, not presented here, are connected with energy losses of metastructure so their effect on the left-handed properties of metastructure could be considered low.

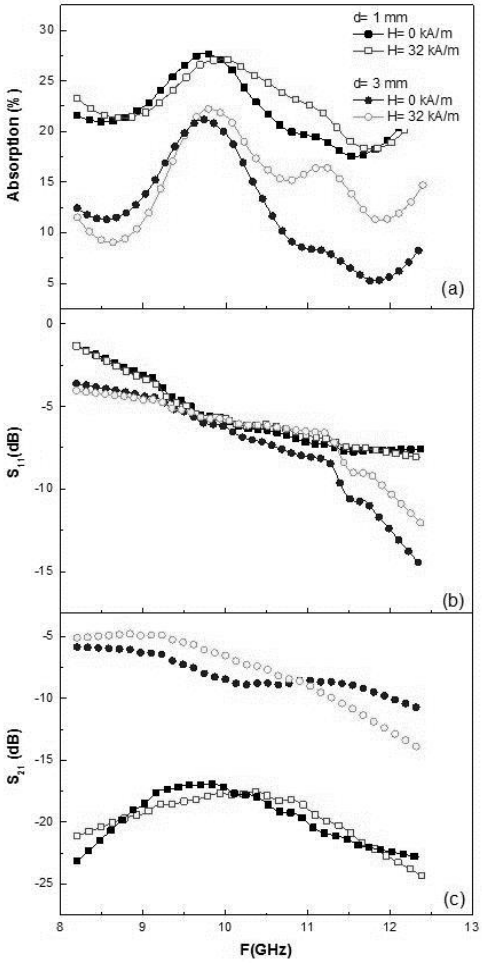

Fig. 6. Absorption frequency dependence (a), calculated using measured coefficients reflexion, S_{11}, (b), and transmission, S_{21}, (c) of the CDNMWs -based metastructure.

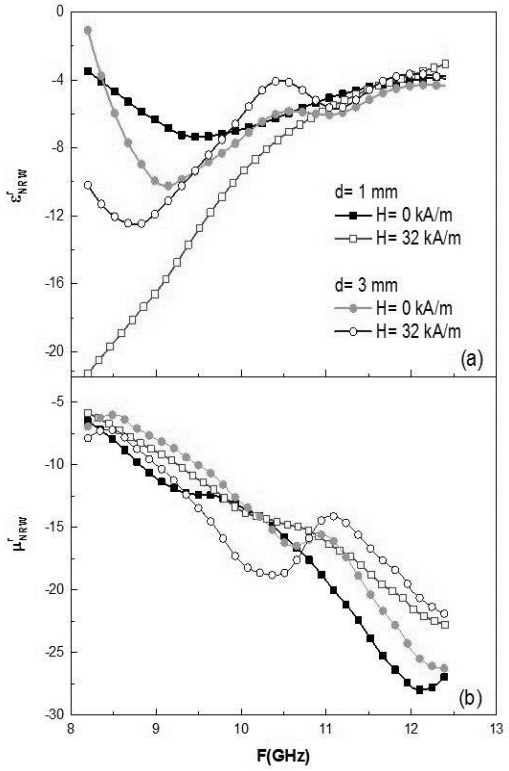

Figure 7. Calculated frequency dependence for ε^r_{NRW} (a) and μ^r_{NRW} (b) of the metastructure based on CDNMWs with Dm = 60 μm.

The negative values of the real part of the dielectric permittivity and magnetic permeability, respectively, confirm that the metastructure presents a left-handed behavior between 8.2 and 12.4 GHz. Also, the peaks appearance at higher frequencies could be ascribed to the long-range dynamic dipole-dipole interactions between the inter-wires.

4. CONCLUSIONS

Experimental and theoretical investigations on the left-handed properties dependence versus the interwire distance of new proposed $Fe_{73.5}Cu_1Nb_3Si_{13.5}B_9$ cold-drawn monocrystalline magnetic microwires - based metastructures in the frequency range 8.2 ÷ 12.4 GHz are presented. The numerical calculations using Nicolson–Weiss–Ross algorithm are in agreement with the experimental results confirming the existence of the left-handed properties of proposed metastructures.

The metastructures with the inter-wire distance of d = 1 mm present a microwave absorption window of about 2 GHz, while the metastructures with the inter-wire distance of d = 3 mm present a microwave absorption window of about 3 GHz, both with the central frequency at about 9.7 GHz. The variation of the interwire distance proves to be a useful tool to obtain metastructures with suitable left-handed characteristics for GHz applications. The properties of such metastructures are found dependent on their geometrical parameters and also on the intrinsic properties of the used microwires, offering flexibility for achieving different engineering requirements.

Acknowledgements. Financial support from NUCLEU Programme - Contract No. 18N/01.01.2023, project PN 23 11 01 01 is highly acknowledged.

REFERENCES

1. N. F. Colaneri and L. W. Shacklette, IEEE Trans. Instr. Meas. **41**, pg. 291-297 (1992).
2. A. N. Yusoff , M. H. Abdullah, S. F. Jusoh, S Ahmad, J.Appl. Phys. **92**, pg. 876882 (2002).
3. R.Walser, *Electromagnetic metamaterials*; Proc. SPIE 4467, Complex Mediums II: Beyond Linear Isotropic Dielectrics vol. **1**, (2001**)**.
4. J.Y. Rhee, Y.J. Yoo, K.W. Kim, Y.J. Kim, Y.P. Lee, J. Electromagnet. Wave **28**, pg. 1541–1580 (2014).
5. H. Guan, D.D.L. Chung, Carbon **157**, 549-562 (2020).
6. I. Kovacic, Z. Rakaric, Z. Kanovic and Y. Rajs, Front. Phys. **10**, 934998 (2022).
7. H. Li, L. Hua Yuan, B. Zhou, X. P. Shen, Q. Cheng and T. Jun Cui; J. Appl. Phys. **110**, 014909 (2011).
8. Li-Hao Zhu, M.-R. Shao, R.-W. Peng, R.-H. Fan, X.-R. Huang, and M. Wang; Opt. Express **21**, pg. A313–A323 (2013).
9. Y.L. Xu, A. Uddin, D. Estevez, Y. Luo, H.X. Peng, F.X. Qin; Composites Science and Technology **189**, 108022 (2020).
10. R.K. Mishra, R.D. Gupta, S. Datar; Plasmonics **16**, 2061–2071 (2021).
11. J. Zhu, Z. Ma, W. Sun, F. Ding, Q. He, Lei Zhou, and Yungui Ma,; Appl. Phys. Lett. **105**, 021102 (2014).
12. F. Capolino, M. Khajavikhan and A. Alu; Appl. Phys. Lett. **120**, 060401 (2022).
13. H. Garcia-Miquel, J. Carbonell, V.E. Boria, J. Sanchez-Dehesa; Appl. Phys. Lett. **94**, 054103 (2009).
14. M. Vasquez, A.L. Adenot-Engelvin; J. Magn. Magn. Mater. **321**, 2066–2073 (2009).
15. H. Ji, G.L. Dai, Y.J. Chen, H.Y. Zhang, Z. Chen, N. Wang, H. Xiao; J. of All. and Comp. **911**, 164904 (2022).
16. X. Qin, H.X. Peng, M.H. Phan, L.V. Panina, M. Ipatov, A. Zhukov; Sensors Actuat. A: Phys. **178**, 118-125 (2012).
17. G. Ababei, C.S. Olariu, N. Lupu, and H. Chiriac; J. Appl. Phys. **117**, 17A502 (2015**)**.
18. J.B. Pendry, A.J. Holden, W.J. Stewart, and I. Youngs; Phys. Rev. Lett. **76**, 4773-4776 (1996).

19. Q. Jiang, C. Xiang, Y. Luo, L. Wu, F. Qin, Y. Jiao, L. Chen, J.-H. Lin; Journal of Materials Research and Technology **9**, 4593-4603 (2020).
20. H. Chiriac, S. Corodeanu, A. Donac, V. Dobrea, G. Ababei, G. Stoian, M. Lostun, T.A. Ovári, N. Lupu; J. Appl. Phys. **117**, 17A314 (2015).
21. H.X. Peng, F.X. Qin, M.H. Phan, Jie Tang, L.V. Panina, M. Ipatov, V. Zhukova, A. Zhukov J. Gonzalez.; Journal of Non-Crystalline Solids **355**, pg. 1380-1386 (2009).
22. H. Garcia-Miquel, J. Carbonell, and J. Sanchez-Dehesa; J. Appl. Phys. **111**, 063901 (2012).
23. A.M. Nicolson, G.F. Ross; IEEE T. Instrum. Meas. **19**, 377 (1970).
24. E. J. Rothwell, J.L. Frasch, S. M. Ellison, Pr. Chahal and R. O. Ouedraogo; Prog. In Electr. Res. **157**, 31-47 (2016).
25. Q. Jiang, C.J. Xiang, Y. Luo, L. W. Wu, Q. Zhang, S.L. Zhao, F.X. Qin, J.H. Lin; Materials & Design **185**, 108270 (2020).
26. W.B. Weir; Proc. IEEE **62**, 33 (1974).
27. G. Ababei, C. S. Olariu, N. Lupu, and H. Chiriac; AIP Advances **6**, 055901 (2016).
28. J. Baker-Jarvis, M.D. Janezic, J.H. Grosvenor, R.G. Geyer; NIST Project, Boulder, CO, Tech. Note 1355, (1992).
29. E. Rothwell, J. Frasch, S. Ellison, P. Chahal, R. Ouedraogo; Progress In Electromagnetics Research **157**, 31-47 (2016).
30. S. Sahin, N. K. Nahar, K. Sertel; IEEE Transactions on Terahertz Science and Technology **10**/4, 404-410 (2020).